Local structure in $Zn_{1-x}Mn_xSe$ alloys

1992 J. Phys.: Condens. Matter 4 1895

(http://iopscience.iop.org/0953-8984/4/8/005)

J. Phys.: Condens. Matter 4 (1992) 1895–1904. Printed in the UK

Local structure in $Zn_{1-x}Mn_xSe$ alloys

Matthew R Weidmann, Jeffrey R Gregg and Kathie E Newman
Department of Physics, University of Notre Dame, Notre Dame, IN 46556, USA

Received 23 May 1991, in final form 23 October 1991

Abstract. A theory of elastic strain relaxation is developed for ternary semiconductor alloys $A_{1-x}B_xC$ with bond length mismatch. The theory is applied to the problem of local structure in $Zn_{1-x}Mn_xSe$ using two models that separately consider random and ordered cation-site occupation. Comparison of results from the models with experimental data for the local structure suggests that the alloy is random and that both anion and cation sublattices relax.

1. Introduction

The structural properties of semiconductor alloys and compounds are fundamental to a general understanding of such systems and to a description of more practical aspects such as electronic or vibrational properties. The structure of a multinary alloy or compound has two components, the long-range order, or Bravais lattice, and the local arrangement of atoms in the unit cell. The Bravais lattice determines the symmetry of the crystal and the shape of the Brillouin zone, while the local structure involves short-range properties such as the near-neighbour coordination and bonding. The importance of details in the local structure has long been recognized in certain classes of semiconductor compounds, notably the chalcopyrites [1]. More recently, the study of local structure has been extended to more common semiconductor systems such as ternary III–V and II–VI alloys of the type $A_{1-x}B_xC$. On first examination, the structural properties of these alloys appear simply related to those of the parent binary compounds AC and BC. The long-range crystalline order observed is on average identical to that of the parent compounds, either cubic-symmetry zinc blende or hexagonal-symmetry wurtzite. The lattice constants of these alloys are generally found to follow Vegard's law—a linear variation between the parent compound values. The local structure suggested by this would be a simple interpolation of the perfect crystal arrangements of the binary compounds, which is the well known virtual-crystal approximation (VCA). However, recent experiments using EXAFS (extended x-ray absorption fine structure) [2–4] clearly show that atoms deviate locally from perfect crystal positions, with first- and second-neighbour distances approaching their separate binary values rather than following the linear variation of the lattice constant. These local distortions within the long-range crystal lattice are due to the relaxation of internal microscopic strain resulting from atomic size mismatch of the alloy constituents.

The purpose of this paper is to present a theoretical study of the origin of local structure observed in recent EXAFS experiments on diluted magnetic semiconductors. Measurements performed on the common-anion alloy $Zn_{1-x}Mn_xSe$ [4] show that

0953-8984/92/081895+10$04.50

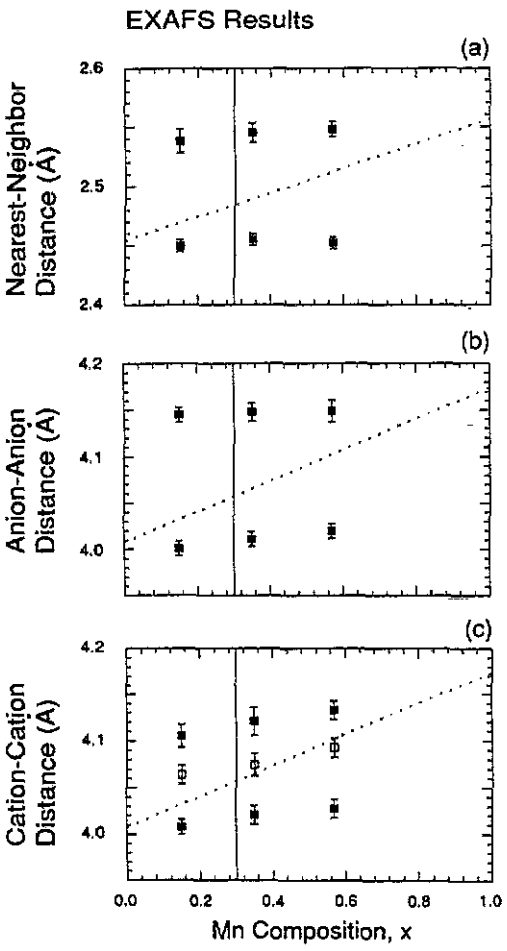

Figure 1. EXAFS results from [4]: (*a*) Zn–Se (lower squares) and Mn–Se (upper squares) bond lengths; (*b*) Se–Zn–Se (lower squares) and Se–Mn–Se (upper squares) anion–anion distances; and (*c*) Zn–Zn (lower full squares), Zn–Mn (middle open squares) and Mn–Mn (upper full squares) cation–cation distances. The broken lines indicate VCA predictions for NN and NNN distances. The vertical lines mark the zinc blende to wurtzite transition at $x \simeq 0.3$.

the near-neighbour (NN) Zn–Se and Mn–Se bond lengths and next-nearest-neighbour (NNN) Se–Zn–Se and Se–Mn–Se anion–anion distances remain nearly constant as a function of composition x, even through the zinc blende to wurtzite phase transition (figures 1(*a*) and 1(*b*)). The NNN cation–cation distances split into three distinct groups: long Mn–Se–Mn, intermediate Mn–Se–Zn, and short Zn–Se–Zn (figure 1(*c*)). This splitting is a prominent feature of the II–VI system not seen in III–V alloys. X-ray diffraction measurements show that the lattice constant of the alloy closely follows Vegard's law [5]. Clearly both the anion and cation sublattices experience significant short-range distortions, which a theoretical description should include.

The theoretical approach taken here combines a simple formalism for the microscopic strain of the alloy with two models of local structure. The relaxation of the cation sublattice is dependent on the NNN environment (NNs being identical anions) and thus it is important to consider different possible cation distributions. The first model uses a set of perfectly ordered structures with extended unit cells as the basis for local atomic arrangements. The second considers a basis of local clusters in an averaged random environment. Predictions of the two models are directly compared with experimental results to clarify trends.

2. The strain energy

The first step in building the theory is to choose a form for the internal elastic strain-energy of the system. The model used here is one of discrete microscopic strain based on the sp^3 bonds common to semiconductors of interest in this work. Such a method permits a simple physical interpretation of forces and parameters and eliminates the need to develop a continuum or effective medium model. We follow Keating [6] and Harrison [7] in resolving interatomic forces into a valence force field. We consider an approximation using only first-neighbour bond-stretching forces and second-neighbour bond-bending forces. The radial force constant C_0 and angular constant C_1 are empirical parameters obtained from the macroscopic elastic constants of the solid. Values used for ZnSe and MnSe appear in table 1. The strain-energy is written as a sum over distorted bonds and angles:

$$E_{\text{strain}} = \sum_{ij} \tfrac{1}{2} C_0 \left(\frac{d_{ij} - d_0}{d_0} \right)^2 + \sum_{ijk} \tfrac{1}{2} C_1 (\delta\theta_{ijk})^2. \tag{1}$$

Here d_{ij} is the distorted bond length, d_0 is the natural bond length (table 1) and $\delta\theta_{ijk}$ is the deviation of the angle from perfect tetrahedral. The radial sum is over each first-neighbour pair and the angular sum is over all unique anion- and cation-centred angles. The advantage of the valence force field is that it allows explicit use of local atomic configurations. Atoms become sites in a classical elastic network. The atoms are allowed to relax to positions determined by minimizing the total strain-energy. In this work, atomic displacements are assumed to be small and are treated with a linear first-order approximation. The final strain-energy, bond lengths and other structural information are obtained from the relaxed configuration of the network.

Table 1. Valence force-field constants C_0 and C_1 (in eV) and natural bond lengths d_0 (in ångstroms) used in the theory for both zinc blende and wurtzite.

Compound	d_0	C_0	C_1
ZnSe	2.454	43.2	1.1
MnSe	2.556	38.0	0.4

The $Zn_{1-x}Mn_xSe$ alloy presents two complications to the use of the valence force field. Most importantly, binary MnSe does not crystallize in the zinc-blende or wurtzite structure in bulk form, but rather in the rock-salt structure. A tetrahedral bond length obtained by extrapolating lattice-constant data from three $A_{1-x}Mn_xSe$ alloys (with A ≡ Zn, Cd, Hg) [5] is used as the natural MnSe bond length for both cubic and hexagonal symmetries. The macroscopic elastic constants for this hypothetical tetrahedral MnSe are estimated from data for the elastic constants of the $Zn_{1-x}Mn_xSe$ alloy [8]. We follow Martin [9] and assume that the reduced elastic constants, $(d^4/e^2)C_{ij}$ (where d is the NN distance and e is the electron charge) will have a linear dependence on the bond ionicity. For the alloy this implies a linear variation with the composition x. An extrapolation based on a least-squares fit of the alloy elastic constant data obtains values for MnSe constants with errors of a few percent. The small uncertainties in the force constants arising from this are no larger than typical errors in experimentally obtained elastic quantities and should

have no noticeable effect on the general trends of interest here. The data for the cubic phase of the alloy are not complete enough for extrapolation to $x = 1.0$, so we only obtain hexagonal elastic constants. This brings in the second complication, that is the alloy undergoes a structural phase transition from zinc-blende to wurtzite at $x \simeq 0.3$, and cannot be grown in bulk above $x \simeq 0.57$. The force constants for the hexagonal case are obtained by using Martin's transfomations [10] to obtain 'effective' cubic elastic constants from the estimated hexagonal constants, and then the microscopic force constants are fit as in Harrison [7]. A small correction due to long-range Coulomb interactions is also included [9]. Since experimental values for the cubic elastic constants of MnSe are not available, we follow Martin [10] in assuming that the average tetrahedral forces in wurtzite and zinc blende are the same and use the same microscopic force constants as in the hexagonal case. Similarly for ZnSe, cubic and hexagonal force constants are obtained from the experimental cubic elastic constants. If experimental data were available for the elastic constants of MnSe and ZnSe for both zinc-blende and wurtzite structures, there would probably be small differences in the microscopic force constants for the two symmetries. Again, this should have little effect on the general trends predicted by the simple empirical theory used here.

3. Ordered structures

The first model of local structure tests the possibility of incipient ordering in the alloy. The crystal lattice is assumed to have a periodic structure with a unit cell larger than that of the parent zinc blende or wurtzite, but still finite. Since the ordering occurs on the cation sublattice, the underlying reference lattice is face-centred cubic (FCC) or hexagonal close packed (HCP). The particular ordered structures considered are the special-k point structures for a FCC or HCP lattice expected to be stable under long-range composition fluctuations according to the Landau–Lifshitz theory of phase transitions, for a review, see [11]. For the FCC case there are a total of five structures occurring at compositions $x = \frac{1}{4}, \frac{1}{2}, \frac{3}{4}$ [12]. There are more structures in the lower-symmetry HCP case, a total of fifteen at compositions $x = \frac{1}{6}, \frac{1}{4}, \frac{1}{3}, \frac{1}{2}, \frac{2}{3}, \frac{3}{4}, \frac{5}{6}$ [13, 14]. Examples of cubic- and hexagonal-symmetry ordered structures appear in figures 2 and 3 [15].

The procedure for finding the minimum strain-energy configuration of the structures is identical to that in [12]. First, coordinates for the positions of the atoms in the primitive cell of each ordered structure are specified. In each case there is an obvious symmetry-allowed distortion which best accommodates the bond-stretching and bond-bending forces. For example, in the chalcopyrite structure, figure 2, the positions of the eight basis atoms are described by just three parameters: the dimensions a and $2c$ of the body-centred tetragonal unit cell and an internal distortion variable p [12]. These three parameters are related back to the dimension a_0 of the underlying reference face-centred cube, $a \simeq c \simeq p \simeq a_0$. In the next step of the calculation, all contributions to equation (1) from all atoms in the basis of the ordered structure are tabulated (without double counting). Then the strain-energy is minimized with respect to all free parameters, thus determining both the positions of all atoms as well as the size of the strain-energy.

The EXAFS measurements for $Zn_{1-x}Mn_xSe$ were performed on samples prepared by the high temperature Bridgman method and long-range crystalline order was not

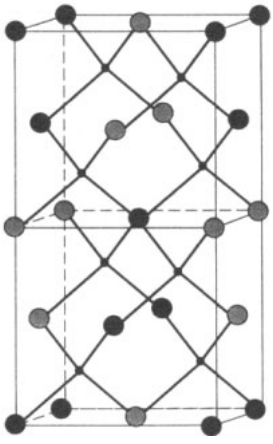

Figure 2. The unit cell of the zinc-blende-derived ordered structure chalcopyrite, ABC_2. Small circles represent anions C, larger circles represent the two types of cations A and B.

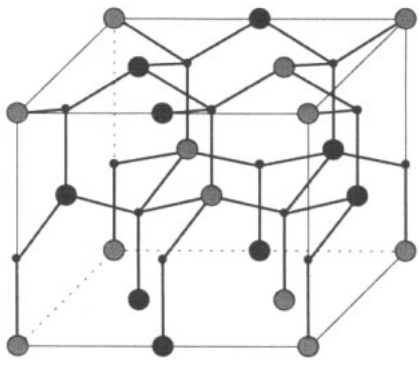

Figure 3. The unit cell of the $BeSiN_2$ structure [15], a wurtzite-derived ordered structure which is a hexagonal analogue of chalcopyrite, shown here for a compound ABC_2. Small circles represent anions C, larger circles represent cations A and B.

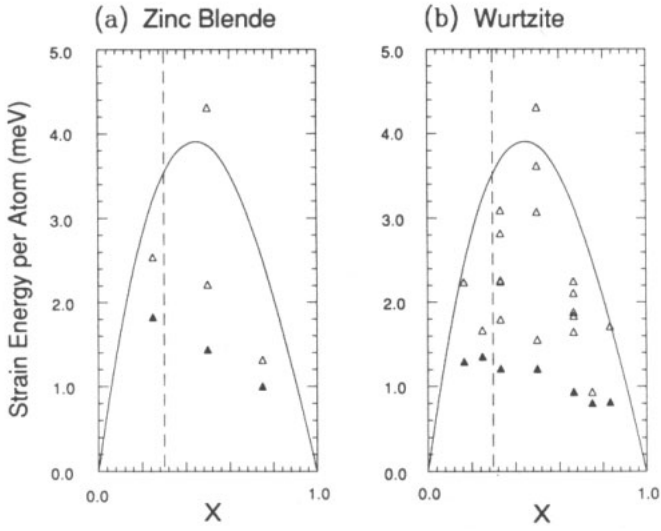

Figure 4. Calculated total strain-energy for $Zn_{1-x}Mn_xSe$ (*a*) cubic and (*b*) hexagonal ordered structures (triangles) and the random alloy (curves). Full triangles indicate the low strain-energy structures. The random and ordered results are shown in the same plots for purposes of comparison only; the two calculations are not directly related. The energy of the random alloy in the zinc-blende and wurtzite structures is identical due to approximations used in the theory. Results are shown for all x for both cubic and hexagonal symmetries for continuity. The location of the phase transition at $x \simeq 0.3$ is indicated.

detected by x-ray diffraction [4]. Our strain model results for the ordered structures can be interpreted in terms of the experimental alloy by speculating that the alloy is microcrystalline, with random orientation of ordered domains. The domains would

have to be large enough that boundary effects would be negligible, since our calculation assumes perfect crystals. The results of the total strain-energy calculations appear in figure 4. The ordered structures group into low-, medium- and high-strain families [14]. Interestingly, the energies of the low-strain hexagonal structures near the phase transition ($x = \frac{1}{4}, \frac{1}{3}$) are almost 0.5 meV (per atom) lower than those of the cubic structure ($x = \frac{1}{4}$). This difference is due purely to the change in symmetry since the force constants used in the two cases are the same. The jump in energy is particularly pronounced because of the large mismatch of angular force constants between ZnSe and MnSe—for an idealized alloy with equal angular force constants, the energy difference is much smaller. This simple empirical model of strain certainly cannot explain the phase transition by itself (and we are dealing only with ordered structures here), but it is tempting to speculate that strain relaxation does play a role.

We expect the low-strain structures to predominate if the system is driven by strain relaxation. In any case, the trends in local structure are the same for all strain families. Results for the NN bond lengths and NNN anion–anion distances for both cubic- and hexagonal-symmetry low-strain structures appear in figures 5(*a*,*b*) and 6(*a*,*b*). Both the bond lengths and anion–anion distances are clearly bimodal, but show a greater change as a function of composition than the experimental results.

The most interesting results are the NNN cation–cation distances, shown in figures 5(*c*) and 6(*c*). Unlike the EXAFS results, the calculated cation–cation distances do not split into three widely separated groups but instead closely follow Vegard's law. This trend is an unavoidable consequence of ordering. If the alloy is to order, it is necessary for the interaction between adjacent cations to be such that atoms of Zn prefer to be surrounded by atoms of Mn, and Mn by Zn ('antiferromagnetic'). The other possible interaction ('ferromagnetic') would lead to clustering of like atoms and phase separation. Thus in all of the ordered structures considered here cations are isolated from other cations of the same type. In fact, in the structures with $x \leqslant \frac{1}{4}$ (or $x \geqslant \frac{3}{4}$) all twelve neighbours of the lower composition cation are of the opposite type. This allows the intervening anions to move easily to accommodate the two natural bond lengths of the alloy, but it also prevents the isolated cation from moving within the unit cell because there is no preferred direction for relaxation. The more common cation also has no reason for motion relative to its neighbours because the less common cations are distributed symmetrically due to the long-range order. Cation positions will relax along with changes in the lattice constants, but distortions internal to the unit cell are largely ruled out. Any alloy that is ordered in the sense defined here will have mean NNN cation–cation distances that closely follow Vegard's law. The conclusion arrived at on the basis of the NNN data must be that the alloy $Zn_{1-x}Mn_xSe$ shows no signs of ordering in the bulk.

4. Random iterative cluster model

Since ordering has proven inadequate for describing the NNN environment of the alloy, a random iterative cluster model (RICM) has been developed to deal with the more conceptually difficult problem of simulating random occupation of the cation sites. The model is an extension of an idea originally proposed by Balzarotti *et al* [3], in which they considered the relaxation of anion-centred tetrahedral clusters with the cation sublattice held fixed. We retain the local-cluster perspective of that approach but also allow the cation sublattice to relax by including cation-centred

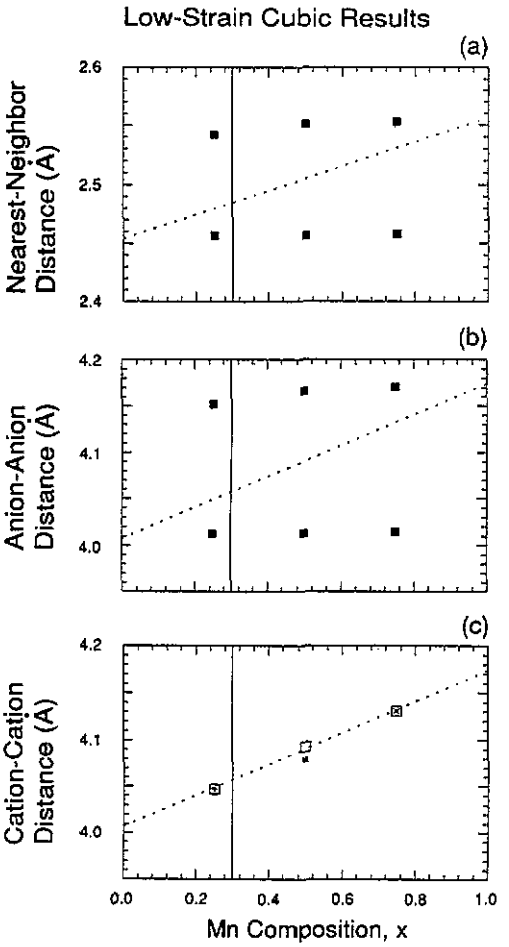

Figure 5. Calculated local structure results for low strain-energy cubic ordered structures: (*a*) Zn–Se (lower squares) and Mn–Se (upper squares) bond lengths; (*b*) Se–Zn–Se (lower squares) and Se–Mn–Se (upper squares) anion–anion distances; and (*c*) Zn–Zn (+), Zn–Mn (open squares) and Mn–Mn (X) cation–cation distances. Results are shown for all values of x for continuity. Note not all types of cation–cation distance are seen at $x = \frac{1}{4}, \frac{3}{4}$.

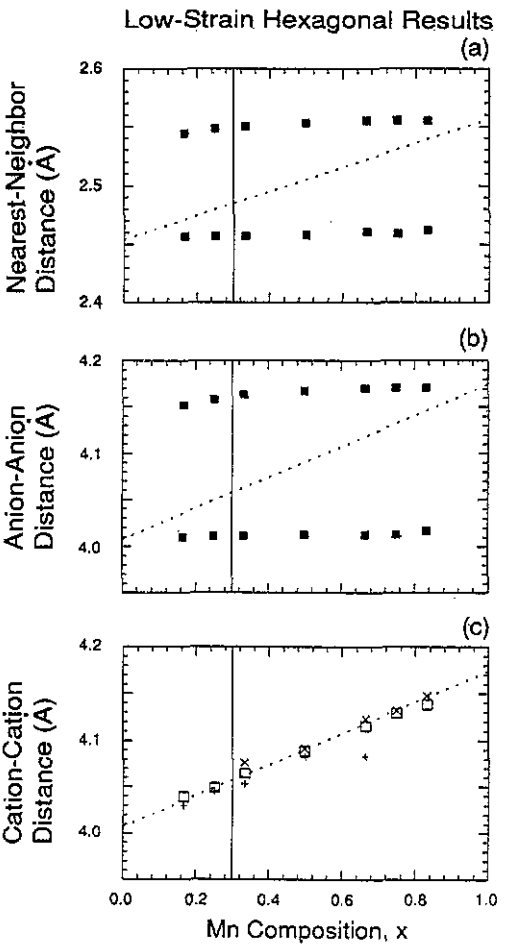

Figure 6. Calculated local structure results for low strain-energy hexagonal ordered structures: (*a*) Zn–Se (lower squares) and Mn–Se (upper squares) bond lengths; (*b*) Se–Zn–Se (lower squares) and Se–Mn–Se (upper squares) anion–anion distances; and (c) Zn–Zn (+), Zn–Mn (open squares) and Mn–Mn (X) cation–cation distances. Results are shown for all values of x for continuity.

clusters via an iteration scheme. Adding cation clusters greatly increases the number of configurations sampled and allows sites on both sublattices to relax in response to neighbours in the second as well as first shell. Thus the model is able to describe the NNN distances that the EXAFS data [4] and ordered model have shown to be important.

The basic building block of the model is the anion-centred cluster. Each anion is surrounded by four cations, each of which can be either Zn or Mn, leading to a total of 16 (2^4) clusters. The more complicated cation-centred clusters are constructed

from four anion clusters that share the common central cation. The four anions are identical, all Se, but there are twelve cations in the second neighbour shell, giving 8192 (2^{13}) total cation configurations. In all clusters, the central atom is relaxed with NNs held fixed. This approximation makes cubic and hexagonal symmetries indistinguishable. The strain-energy terms used include the four bonds and six angles originating on the central atom. The correct counting of energy terms for a zinc-blende or wurtzite structure gives two bonds and six angles per atom, so the radial terms acquire an extra factor of $\frac{1}{2}$ to avoid double counting of bonds. Angles centred on the NNs of the central atom are not directly included but dealt with in later steps of the iteration process when the other sublattice is relaxed.

The relaxation scheme begins with all atoms on an undistorted lattice with the lattice constant for a given composition determined by Vegard's law. The iteration is accomplished by using relaxed positions of central atoms in a given step to determine the distorted positions of surrounding atoms in the next step. Necessarily, the anion clusters are relaxed first. The distorted anion clusters are used to build cation clusters in which tetrahedral symmetry is now broken. The full set of cation configurations is then relaxed and the iteration returns to the anion clusters with a composition-weighted binomial averaging over the 8192 cation clusters that reduces the number of configurations to 16. This averaging procedure allows a given atom at the centre of a cluster to respond explicitly to three of twelve second neighbours and 'smooths out' the cation relaxation. The averaging also places symmetry restrictions on the relaxation of the anions. All clusters with the same number of cations of a given type are rotationally equivalent, so there are only five independent anion clusters, not 16. (The five clusters are Zn_4, Zn_3Mn, Zn_2Mn_2, $ZnMn_3$, and Mn_4.) The iteration converges quickly, with atomic positions stabilized to the level of one part in 10^8 in approximately 20 steps. Structural information such as NN and NNN distances, distributions for these, and the strain-energy are extracted from composition-weighted averages over the final forms of the distorted clusters.

The random iterative cluster model has some systematic properties that should be mentioned. The iteration procedure allows atoms to occupy distorted positions around the perfect crystal sites of the original lattice, but does not allow the underlying lattice itself to distort. Thus the overall mean NN and NNN distances (not separated according to type) are forced to obey Vegard's law. The model also shares some properties with a theory of a random elastic network with a length mismatch developed by Thorpe and Garboczi [16]. Thorpe and Garboczi consider pure radial forces on the two-dimensional triangular net and find an interesting result in the NN environment for the special case of equal force constants, namely the short and long bonds have linear mean lengths and identical shapes of distributions as a function of composition x. Angular forces must be included to stabilize the zinc-blende lattice, so we study the case $C_0^A = C_0^B$, $C_1^A = C_1^B$. The RICM does produce linear NN distances and identical distribution shapes in this instance, illustrating the similarities of the theories. Histogram plots of the NN distributions for three compositions appear in figure 7. Additionally, the RICM predicts both linearity and identical distribution shapes to extend to NNN distances.

Application of the random iterative cluster model to $Zn_{1-x}Mn_xSe$ reproduces qualitative trends in both NN and NNN environments. Because of the approximations of rigid NN relaxation and equal zinc-blende and wurtzite force constants, the model does not distinguish cubic and hexagonal symmetries. This has little consequence for trends in local structure, if the ordered structure results are a guide, although it is

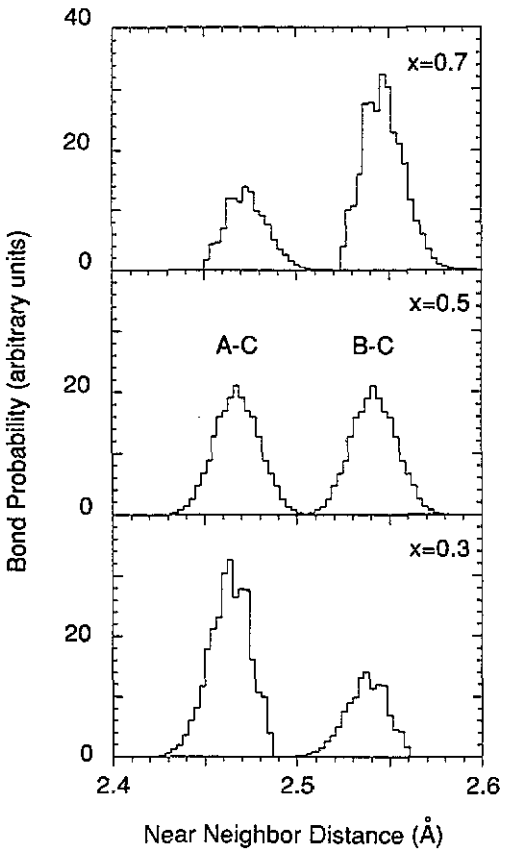

Figure 7. Calculated NN bond-length distributions from the random iterative cluster model for the alloy $A_{1-x}B_xC$ with $C_0^A = C_0^B = 40.0$ eV, $C_1^A = C_1^B = 1.0$ eV (values typical of II–VI materials). The natural A–C and B–C bond lengths are taken to be the same as Zn–Se and Mn–Se, respectively. At a given composition, the short and long bond-length distributions have identical shapes after vertical scaling.

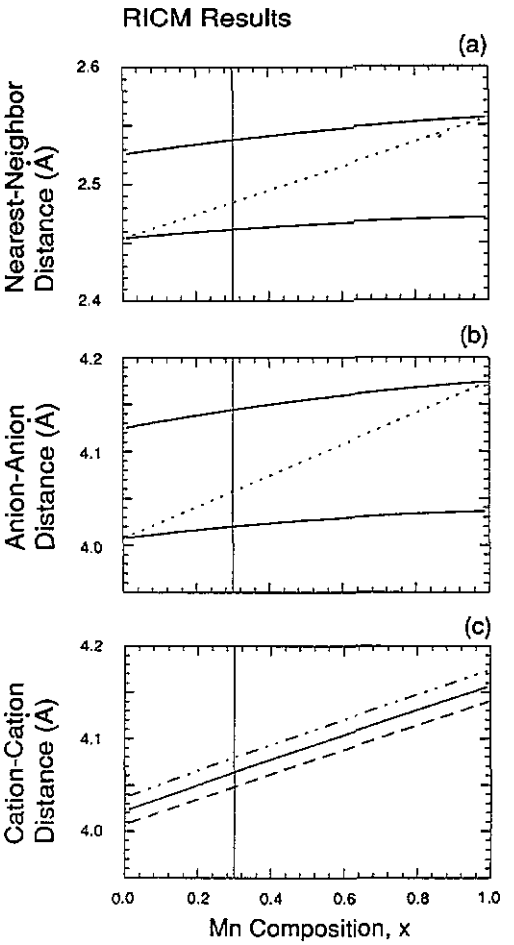

Figure 8. Calculated local structure results from the random iterative cluster model: (*a*) Zn–Se (lower curve) and Mn–Se (upper curve) bond lengths; (*b*) Se–Zn–Se (lower curve) and Se–Mn–Se (upper curve) anion–anion distances; and (*c*) Zn–Zn (broken curve), Zn–Mn (full curve) and Mn–Mn (chain curve) cation–cation distances. Cubic and hexagonal symmetries are not distinct. The predicted VCA distance is not shown.

unfortunate that we cannot calculate distinct total strain energies for the two cases using the RICM. The strain-energy (identical for zinc blende and wurtzite) is plotted as a function of composition in figure 4. Results for the mean Zn–Se (short) and Mn–Se (long) bond lengths appear in figure 8(*a*), along with the calculated Se–Zn–Se and Se–Mn–Se anion–anion distances in figure 8(*b*). As with the ordered-structure results, both sets of distances are similar to the experimental data but with more change as a function of composition x. The slight curvature is caused by the mismatch of the force constants. Interestingly, the predicted mean cation–cation distances, figure 8(*c*), mimic the experimental trend and split into three distinct groups, Mn–Mn (long), Mn–Zn (intermediate), and Zn–Zn (short). However, the calculated cation–cation distances approach Vegard's law much more closely than the experimental results.

This perhaps indicates that the alloy is random but the model is too limited to describe the trends fully. Small cluster size, symmetry imposed restrictions on relaxation, and the two force-constant approximation could all be important limitations of the model. Nevertheless, the model has been instructive in clarifying experimental trends.

5. Summary

A simple theory of elastic strain has been applied to the problem of alloy relaxation due to length mismatch in $Zn_{1-x}Mn_xSe$. Contrasting results from two models of local structure, it is found that a model based on a random cation distribution give a good qualitative description of both the NN and NNN environments as determined by experiment, while a model based on long-range ordering fails. In particular, the random model predicts a trimodal splitting of the NNN cation–cation distances, a prominent feature of the local structure observed experimentally in this II–VI system. This success serves to emphasize the importance of both the cation-site distribution and strain relaxation extending beyond the NN environment in describing local structure in ternary semiconductor alloys.

Acknowledgments

We are grateful for many stimulating discussions with the Notre Dame EXAFS group, especially B A Bunker and R A Mayanovic. We would like to thank M F Thorpe for providing a copy of his work prior to publication. This work was supported by the United States Office of Naval Research under contracts N00014-89-J-1198 and N00014-91-J-1062.

References

[1] Kaufmann U and Schneider J 1974 *Festkörperprobleme* **14** 229
[2] Mikkelsen J C Jr and Boyce J B 1983 *Phys. Rev.* B **28** 7130
[3] Balzarotti A, Motta N, Kiesel A, Zimnal-Starnawska M, Czyzyk M T and Podgorny M 1985 *Phys. Rev.* B **31** 7526
[4] Pong W F, Mayanovic R A, Bunker B A, Furdyna J K and Debska U 1990 *Phys. Rev.* B **41** 8440
[5] Yoder-Short D R, Debska U and Furdyna J K 1985 *J. Appl. Phys.* **58** 4056
[6] Keating P N 1966 *Phys. Rev.* **145** 637
[7] Harrison W A 1980 *Electronic Structure and the Properties of Solids* (San Francisco: W H Freeman) ch 8
[8] Mayanovic R A, Sladek R J and Debska U 1988 *Phys. Rev.* B **38** 1311
[9] Martin 1969 *Phys. Rev.* B **1** 4005
[10] Martin R M 1972 *Phys. Rev.* B **6** 4546
[11] de Fontaine D 1979 *Solid State Physics* ed H Ehrenreich, F Seitz and D Turnbull (New York: Academic)
[12] Newman K E, Shen J and Teng D 1989 *Superlattices and Microstructures* **6** 245
[13] Kudō T and Katsura S 1976 *Prog. Theor. Phys.* **56** 435
[14] Gregg J R and Newman K E unpublished
[15] Parthé 1964 *Crystal Chemistry of Tetrahedral Structures* (New York: Gordon and Breach)
[16] Thorpe M F and Garboczi E J 1990 *Phys. Rev.* B **42** 8405